Molecular dynamic simulation of mechanical behaviour of RGO produced by thermal reduction method

Xia Liu ✉, *Qingsheng Yang*

Department of Mechanical Engineering, Beijing University of Technology, Chaoyang, Beijing 100124, People's Republic of China
✉ *E-mail: liuxia@bjut.edu.cn*

Published in Micro & Nano Letters; Received on 9th February 2017; Revised on 29th March 2017; Accepted on 4th April 2017

Chemical oxidation of graphite and subsequent exfoliation allow the large-scale production of isolated graphene oxide (GO), in which the induced oxygen-containing functional groups on GO surface were then removed by means of reduction processes. The residual functional groups including carbonyl, hydroxyl and epoxy groups as well as the newly formed defects, significantly influence the physical properties of reduced GO (RGO). Here, RGO structures were generated through a thermal reduction process of GO using molecular dynamics simulations, in which the transformation of functional groups and the formation of non-hexagonal rings/defects were captured. The results suggested the formation of two RGO structures with different contents of functional groups at C/O ratios of about 11 and 13. These structures were obtained using various durations of the thermal reduction process. The dependence of tensile behaviour of RGOs on the structure and chirality as well as the influence of temperature on the tensile properties of RGOs were also evaluated. It was found that the strength and Young's modulus of RGOs decreased as a result of the residual functional groups and newly formed defects, and were decreased with the environment temperature.

1. Introduction: Graphene materials have attracted tremendous attention in a wide range of areas due to their excellent mechanical, thermal, electrical and optical properties [1–5]. Furthermore, the fact that graphene could easily be produced through the reduction of graphene oxide (GO), this induces diverse structures of reduced GO (RGO) with varied contents of oxygen-containing functional groups including epoxy, hydroxyl and carboxyl groups [6–8]. Nowadays, RGOs are widely applied in various fields such as nanoelectronics [9, 10], sensors [11–13], actuators [14], supercapacitors [15, 16] and transparent conducting thin films [17, 18]. A number of theoretical and experimental investigations have been devoted to gain further insights into the understanding of structural characteristics and mechanical properties of graphene materials. For instance, Lee *et al.* [17] measured the elastic properties and intrinsic strength of free-standing monolayer graphene membranes using nanoindentation atomic force microscopy. They recorded Young's modulus as 1.0 ± 0.1 TPa and intrinsic stress as 130 ± 10 GPa at a strain of 0.25. Chen *et al.* [19] prepared RGO paper by an annealing process and measured the mean Young's modulus and tensile strength as 41.8 GPa and 293.3 MPa, respectively. Robinson *et al.* [20] tuned the frequency response of suspended membranes through a thermal annealing process and obtained Young's modulus of RGO thin films as 185 GPa. Gómez-Navarro *et al.* [21] examined the real space atomic resolution of RGO structures and revealed a remarkable amount of topological defects on RGO sheets after the reduction process. In sum, though graphene membranes with superior mechanical properties could be obtained, Young's modulus for practical RGOs constitutes only a small percentage of expected values, owing to the presence of defects in the carbon sheets.

Since the experimental research processes aiming to explain the relationship between the structure and mechanical properties of RGOs are quite difficult to achieve, atomistic simulation approaches based on density-functional theory (DFT) and molecular dynamics (MDs) have shown their usefulness in addressing the mechanical behaviour of RGOs. For example, Nasehnia *et al.* [22] examined the electronic structure and linear optical properties of oxygen-functionalised graphene using DFT. Zhao and Aluru [23] studied the variation of ultimate strength in graphene as a function of temperature, strain rate and crack length, using MD simulations. Zhang *et al.* [24] estimated Young's modulus, interlayer shear modulus and ultimate tensile strength of bilayer graphene films coupled by sp3 bonding, using MD simulations. Finally, Wang and Zhang [25] calculated the mechanical deformation of a graphene bilayer under in-plane tensile or compressive loadings using atomistic MD simulations. Overall, the above-utilised simulations to estimate Young's modulus and elastic strength agreed well with the experimental data, hence validating the accuracy of atomistic MD simulations. Recently, Fonseca *et al.* [26] confirmed that MD simulations based on reactive force field provide better overall results.

In addition to predicting the mechanical properties of pure graphene, MD simulations are also aimed to clarify how the functional groups affect the structural and mechanical behaviours of RGOs. With respect to this, Paci *et al.* [27] employed MD simulations to examine the behaviour of GOs on heating to room and thermal reduction temperatures. Abolfath and Cho [28] employed MD simulations to study the chemical reduction process of GOs in environments enriched with hydrogen. Both MD and DFT calculations were exploited by Kumar *et al.* [29] to assess the influence of various functional groups on stability, work function and photoluminescence of RGOs. Their results demonstrated a significant tunability in the work function of RGOs up to 2.5 eV when the composition of oxygen-containing functional groups was altered at fixed oxygen concentration. Recently, Dewapriya *et al.* [30] studied the effects of hydrogen functionalisation on fracture strength of RGO using MD simulations and classical continuum concepts. Furthermore, combined effects of functional groups, lattice defects and edges on infrared spectra of GO, were examined by means of first-principle calculations [31]. Wang *et al.* [32] studied the effects of the structural characteristics of GO on the mechanical properties and failure mechanisms along both the armchair and zigzag directions using MD simulations. Wei *et al.* [33] explored the mechanical behaviour of GO sheet subjected to equibiaxial tension using density-functional-based tight-binding modelling. Finally, Lawson and Beregszaszy [34] estimated the binding energies of mono and bilayers graphene sheets coated with up to 24 oxygen atoms sequentially added to one surface of a monolayer and bilayer.

doi: 10.1049/mnl.2017.0072

As discussed above, though atomistic structures of RGOs prepared by thermal and chemical reduction processes were studied by MD simulations, insufficient research still exists with regard to effects of the atomic structure of RGOs on their resulting mechanical behaviours. Owing to the variations in RGO structures arising from differences in the reduction methods, more realistic models integrating the functional groups and lattice defects are required for proper interpretation of the mechanical behaviours of the resulting materials. In this Letter, the atomic-scale structures of realistic RGOs were evaluated by means of atomistic MD simulations in an effort to provide useful insights into the effect of functional groups and lattice defects on the mechanical behaviours of the resulting materials. These results may also help in gaining a better understanding of the RGO thin films.

2. Models and methods: All MD simulations were conducted with an large-scale atomic/molecular massively parallel simulator program [35]. ReaxFF ('reactive force field') was employed to calculate the potential energy of the system in MD simulations. The ReaxFF is a bond-order-based force field developed by Duin *et al.* [36] at the California Institute of Technology. The method employed distance-dependent bond-order functions to display the chemical bonding contributions to the potential energy, and allowing the continuous bond formation/breaking. In this Letter, ReaxFF was used to study the structural evolution of graphene materials at different temperatures, where the qualitative agreement with the experimental data was previously demonstrated [37]. Briefly, the thermal reduction process of GO and mechanical properties of the obtained RGOs at different temperatures were calculated by ReaxFF using both force fields features. The energy terms of the total potential energy for each force field are described below.

First, the total potential energy in ReaxFF force field was computed as the sum of various energy terms

$$E_{\text{total}} = E_{\text{bond}} + E_{\text{over}} + E_{\text{val}} + E_{\text{tors}} + E_{\text{vdW}} + E_{\text{coul}} \quad (1)$$

where E_{bond}, E_{over}, E_{val}, E_{tors}, E_{vdW} and E_{coul} are the respective energies of the bond, over coordination, angle, torsion, van der Walls and Coulomb interactions.

As discussed in previously published MD simulation reports [36, 38], the GO structures formed by carbonyl, hydroxyl and epoxide groups distributed in a disordered manner on basal planes were found to be the best model describing the experimental data. Accordingly, GO structures decorated with disordered carbonyl, epoxy and hydroxyl groups were designed and produced (Fig. 1). The primary GO sheet was 5 nm×5 nm decorated with 30 epoxy groups, 60 carbonyl groups and 45 hydroxyl groups. Hence, the total number of atoms on the GO sheet was 1110 including 930 carbon atoms, 135 oxygens and 45 hydrogens, resulting in a typical C/O ratio range of GO around 6.88 [39]. It is important to note that due to limitations in the simulation timescale, the structural transformation during thermal reduction, as well as the mechanical performance calculated based on MD simulations should be considered qualitative as opposed to quantitative in nature.

3. Results and discussion: Before the reduction process, a preliminary energy minimisation of GO structures with a stopping tolerance of 1×10^{-10} for both force and energy was performed, which then was followed by multistep MD simulations of thermal reduction process of GO. First, the system containing the relaxed GO was further released under periodic boundary condition in a canonical constant temperature and constant pressure (NPT) ensemble with a Nose–Hoover thermostat for temperature control at 300 K and time step of 0.25 fs. During this process, the total number of atoms, system pressure and temperature remained unchanged. The temperature of the system was then raised at a rate of 3 K/ps until reaching 1500 K. Next, the system was maintained for a certain time (100 and 200 ps) at 1500 K to allow the formation of RGO. The NPT ensemble allows control over both the temperature and pressure. The unit cell vectors are allowed to change and the pressure is adjusted by adjusting the volume. This ensemble is chosen because the correct pressure, volume and densities are important in the present simulations.

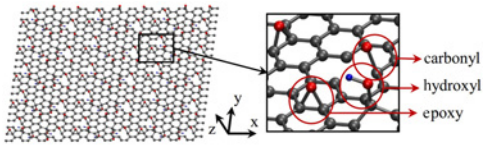

Fig. 1 *Primary GO structure for thermal reduction*

In this Letter, two RGO structures with different reduction degrees named as RGOI and RGOII, were obtained over the thermal reductions of 100 and 200 ps, respectively. Afterwards, the system was cooled down to 300 K at a rate of 3 K/ps over a time interval of 40 ps. Finally, the obtained RGO structures were fully relaxed to confirm stable structures. The detailed vertical views of both RGOI and RGOII structures are depicted in Figs. 2*a* and *b*, respectively. Yet, it should be pointed out that the surface wrinkle degree of RGO sheets was further intensified after the reduction process.

For clear comparisons, the number of functional groups and defects available on primary GO and subsequent RGOs are listed in Table 1. After thermal reduction process, some of the oxygen and hydrogen atoms are exfoliated from the primary molecules and form new molecules, while some of them are exfoliated out of the GO structure. It was shown that the number of carbonyl, epoxy and hydroxyl groups decreased in both RGO structures, leaving room to the formation of a new type of oxygen-containing groups, namely ethers. Furthermore, some non-hexagonal rings and defects emerged in the structures after the thermal reduction process. Since the carbonyl, epoxy and hydroxyl groups have different molecular structures, the numbers of these groups can be counted from the integral structure of the RGO after the reduction process.

By comparing the number of functional groups and defects in RGOI and RGOII, it was found that removal amount of previous oxygen-containing groups and formed groups related ethers,

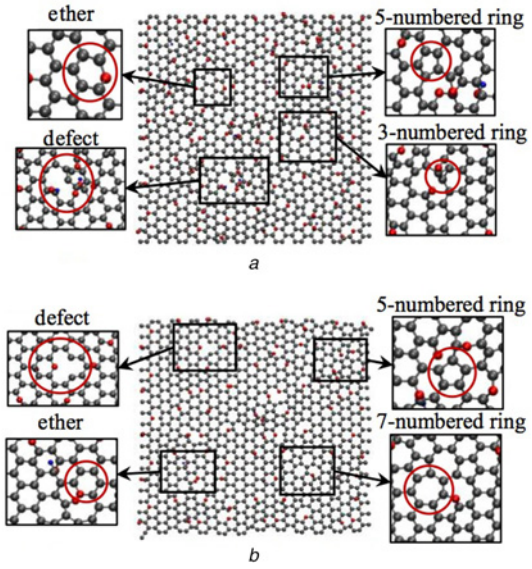

Fig. 2 *Structures of RGO induced by thermal reduction processes over*
a 100 ps
b 200 ps

Table 1a Number of functional groups and defects recorded on GO and RGO surfaces

Type	Atom number	Carbonyl	Epoxy	Hydroxyl
GO	1110	60	30	45
RGOI	1054	35	25	7
RGOII	1016	42	7	1

Table 1b

	Ether	Non-hexagonal ring	Defect
GO	—	—	—
RGOI	20	5	7
RGOII	22	8	13

non-hexagonal rings and defects increased in numbers as the reduction time increased. Briefly, the C/O ratio of RGO rose to 10.98 and 12.92 after reduction periods of 100 and 200 ps, respectively. Previously reported experimental data suggested that GO at C/O ratio of 4 : 1–2 : 1 could be improved to ~12 : 1 after the reduction process [8, 39–41]. Therefore, the C/O ratios of obtained RGO structures were found to agree well with the experimental data.

To study the mechanical behaviour and fracture characteristics of RGOs, tensile tests of primary GO and obtained RGO structures were performed using MD simulations. The tensile tests of pure graphene structures with the same size as RGOs were also simulated to confirm the accuracy of the present simulation method. The deformation controlled uniaxial tensile tests at a strain rate of 0.002 fs^{-1} along both the armchair and zigzag directions of the structures were thus examined. The strain increment is applied to the structure after every 10,000 time steps with the step size of 0.1 fs. It should be noted that the simulated strain rate is several orders of magnitude higher than typical experimental strain rates. This is due to the fundamental limitation on the time scale of MD simulations, but is necessary to obtain significant amount of deformation within a reasonable computation time. Although the strain rate is 5 orders of magnitude higher than the experimental values, the overall characteristics of structures to deformation can be well captured. The velocity-Verlet algorithm is employed to integrate the equations of motion. The pressure component perpendicular to the loading direction is controlled to maintain the uniaxial tensile condition. The dimension of the simulation box along the tensile direction is changed at the constant strain rate, while the dimension along the direction perpendicular to the tensile direction is free to shrink.

The tensile stress of the materials was calculated by dividing the applied load by the cross-sectional area

$$\sigma = \frac{F}{A} = \frac{F}{L \cdot D} \tag{2}$$

where L and D represent the length and thickness (0.34 nm) of RGO, respectively. The total force F is calculated by summing the forces of all atoms on the loaded end. Tensile stress–strain curves of graphene materials along the zigzag and armchair directions are plotted in Figs. 3 and 4.

The Young's modulus, E, can then be calculated by dividing the tensile stress by extensional strain in elastic portion of the stress–strain curve

$$E = \frac{\sigma}{\varepsilon} = \frac{F/LD}{\Delta l/l_0} \tag{3}$$

where l_0 and Δl are the initial length and extension of the material along the tensile direction, respectively. In these curves, the elastic

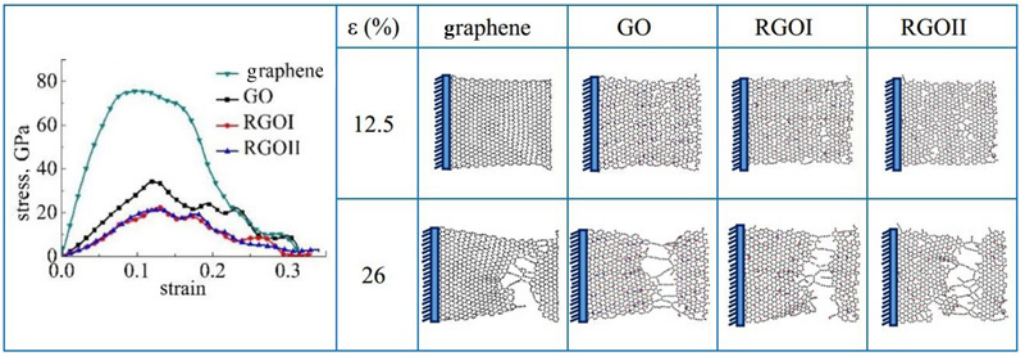

Fig. 3 *Tensile stress–strain curves and fracture morphology of graphene materials under tensile loading along zigzag direction*

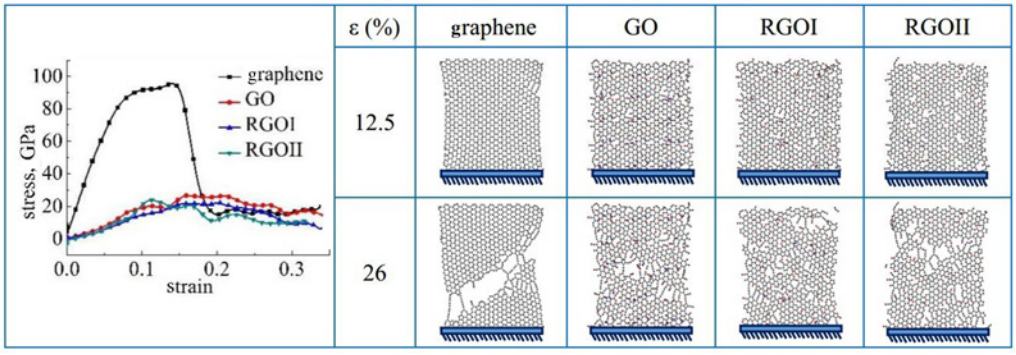

Fig. 4 *Tensile stress–strain curves and fracture morphology of graphene materials under tensile loading along armchair direction*

doi: 10.1049/mnl.2017.0072

Table 2 Tensile strength and Young's modulus of various graphene materials

Type	Strength, GPa		Young's modulus, TPa	
	Zigzag	Armchair	Zigzag	Armchair
graphene	78	96	1.1	1.3
GO	35	29	0.29	0.18
RGOI	23	26	0.15	0.12
RGOII	21	27	0.15	0.12

strain is considered as 0.05. The tensile strength and calculated Young's modulus of graphene materials are listed in Table 2.

The values of the tensile strength of graphene along the zigzag and armchair directions were estimated as 78 and 96 GPa, respectively (Table 2). Meanwhile, the respective Young's modulus values of pure graphene along the zigzag and armchair directions were estimated to 1.1 and 1.3 TPa. These data agreed well with the experimental results [42]. Yet, the oxygen-containing functional groups and defects significantly influenced the tensile properties of GO and RGO. Specifically, the tensile strengths of GO along the zigzag and armchair directions were reduced by, respectively, 55 and 70%, when compared with the tensile strength of pure graphene.

According to the simulation results, the thermal reduction process may also influence the mechanical properties of RGO as additional defects were formed after long periods of thermal reduction. As a result, the tensile strength and Young's modulus of RGO values along the zigzag direction decreased by about 34 and 48%, respectively. By contrast, the tensile strength and Young's modulus of RGO along the armchair direction declined by only 7 and 33%, respectively.

The combined effect of functional groups and defects on the mechanical behaviour of graphene materials were also discussed in terms of deformation and fracture characteristics. The structural evolution and fracture of graphene materials under tensile loading are described in Figs. 3 and 4. For pure graphene structures, extensional strain reaching 12.5% led to the formation of shear band on the graphene sheet, which, in turn, caused the material to yield. At strains of 25%, pure graphene was fractured along the shear band. For GO and RGO structures, extensional strains reaching 12.5% induced enlargement of previous defects, as well as led to the formation of some initiated additional cracks. Afterwards, weak cross-sections took place that resulted in fractures of the carbon sheets with increasing strains.

In the present Letter, the RGO possessed lower tensile properties along the zigzag direction caused by weaker cross-sections under loading. By contrast, RGO structures were fractured by discrete defects under tensile loading along the armchair direction. Therefore, the tensile strengths of RGO structures along the armchair direction were slightly higher than that obtained along the other direction.

The dependence of both the tensile strength and Young's modulus of RGOs on the environment temperature were also examined, and the results are gathered in Fig. 5. In general, the tensile strength and Young's modulus of RGOs decreased as the temperature rose. However, while the elastic strength declined uniformly as a function of temperature, Young's modulus decreased in a two-stage trend.

First, it is found from the curves in Fig. 5*a* that there is an inflection point at temperature of about 1900 K. Then, further simulations at temperatures of 2300 and 2700 K were performed. The strength shows significant decrease relative to the strength at temperature of 1900 K.

Then, as exhibited by Fig. 5*b*, Young's modulus of RGOs decreased slightly as temperature increased up to about 1900 K,

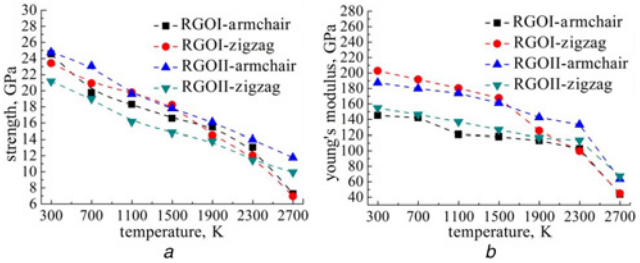

Fig. 5 *Influence of temperature on*
a Tensile strength
b Young's modulus of RGOs

though the critical temperature for RGOI along the zigzag direction was around 1500 K. For instance, when the environment temperature reached 1900 K, Young's modulus of RGOI along the armchair direction was 102 GPa, which was ~30% lower than the value obtained at room temperature. Beyond that, Young's modulus reduced significantly to 44 GPa, suggesting that the material became much weaker at this temperature. Moreover, the tensile strength of RGOI along the armchair direction at 2300 K was estimated to about 47%, which was less than the value registered at room temperature.

4. Conclusion: This account presented the structural evolution characteristics and mechanical behaviour of RGOs using MD simulations. The transformation of oxygen-containing functional groups and formation of non-hexagonal rings and defects were tracked from the evolutionary trajectory of RGO structures during thermal reduction processes. From the obtained RGO structures, it was shown that the number of carbonyl, epoxy and hydroxyl groups decreased after the thermal reduction process, leaving the room for the formation of a new type of oxygen-containing functional groups, namely ethers. Moreover, the removal amount of previous oxygen-containing groups, ether groups, non-hexagonal rings and defects increased in numbers as a function of the reduction time. The C/O ratios of the obtained RGO structures were estimated as 10.98 and 12.92 after reduction periods of 100 and 200 ps, respectively. The effect of residual functional groups on the mechanical behaviour of RGO layers was also analysed. The structural evolutionary trajectory observations revealed the expansion of defects fractures in RGOs. Finally, examination of the dependence of mechanical properties of RGOs on chirality and temperature indicated that the tensile strength and Young's modulus of RGOs decreased as the temperature rose.

5. Acknowledgments: The authors gratefully acknowledge the financial supports to this research work from The National Natural Science Foundation of China (grant nos. 11502007, 11472020) and The Rixin Fund of Beijing University of Technology.

6 References

[1] Allen M.J., Tung V.C., Kaner R.B.: 'Honeycomb carbon: a review of graphene', *Chem. Rev.*, 2010, **10**, pp. 132–145
[2] Choi W., Lahiri I., Seelaboyina R., *ET AL.*: 'Synthesis of graphene and its applications: a review', *Crit. Rev. Solid State*, 2010, **35**, pp. 52–71
[3] Young R.J., Kinloch I.A., Gong L., *ET AL.*: 'The mechanics of graphene nanocomposites: a review', *Compos. Sci. Technol.*, 2012, **72**, pp. 1459–1476
[4] Gomez-Navarro C., Weitz R.T., Bittner A.M., *ET AL.*: 'Transport properties of individual chemically reduced graphene oxide sheets', *Nano Lett.*, 2007, **7**, p. 3499
[5] Yan J.A., Xian L., Chou M.Y.: 'Structural and electronic properties of oxidized graphene', *Phys. Rev. Lett.*, 2009, **103**, p. 86802

[6] Compton O.C., Nguyen S.T.: 'Graphene oxide, highly reduced graphene oxide, and graphene: versatile building blocks for carbon-based materials', *Small*, 2010, **6**, pp. 711–723
[7] Mei X., Meng X., Wu F.: 'Hydrothermal method for the production of reduced graphene oxide', *Physica E*, 2015, **68**, pp. 81–86
[8] Pei S., Cheng H.: 'The reduction of graphene oxide', *Carbon*, 2012, **50**, pp. 3210–3228
[9] Castro E.V., Novoselov K.S., Morozov S.V., *ET AL.*: 'Biased bilayer graphene: semiconductor with a gap tunable by the electric field effect', *Phys. Rev. Lett.*, 2007, **99**, p. 216802
[10] Venugopal A., Colombo L., Vogel E.M.: 'Contact resistance in few and multilayer graphene devices', *Appl. Phys. Lett.*, 2010, **96**, p. 13512
[11] Mohammad Haniff M.A.S., Muhammad Hafiz S., Wahid Z., *ET AL.*: 'Piezoresistive effects in controllable defective HFTCVD graphene-based flexible pressure sensor', *Sci. Rep. UK*, 2015, **5**, p. 14751
[12] Aguilera-Servin J., Miao T., Bockrath M.: 'Nanoscale pressure sensors realized from suspended graphene membrane devices', *Appl. Phys. Lett.*, 2015, **106**, p. 83103
[13] Fardindoost S., Alipour A., Mohammadi S., *ET AL.*: 'Flexible strain sensors based on electrostatically actuated graphene flakes', *J. Micromech. Microeng.*, 2015, **25**, p. 75016
[14] Hu Y., Lian H., Zu L., *ET AL.*: 'Durable electromechanical actuator based on graphene oxide with in situ reduced graphene oxide electrodes', *J. Mater. Sci.*, 2016, **51**, pp. 1376–1381
[15] Zhang J., Zhao X.S.: 'Conducting polymers directly coated on reduced graphene oxide sheets as high-performance supercapacitor electrodes', *J. Phys. Chem. C*, 2012, **116**, pp. 5420–5426
[16] Zhao B., Liu P., Jiang Y., *ET AL.*: 'Supercapacitor performances of thermally reduced graphene oxide', *J. Power Sources*, 2012, **198**, pp. 423–427
[17] Lee D.W., Hong T., Kang D., *ET AL.*: 'Highly controllable transparent and conducting thin films using layer-by-layer assembly of oppositely charged reduced graphene oxides', *J. Mater. Chem.*, 2011, **21**, pp. 3438–3442
[18] Kim S., Joo P., Ahn G., *ET AL.*: 'Transparent conducting films based on reduced graphene oxide multilayers for biocompatible neuronal interfaces', *J. Biomed. Nanotechnol.*, 2013, **9**, pp. 403–408
[19] Chen H., Muller M.B., Gilmore K.J., *ET AL.*: 'Mechanically strong, electrically conductive, and biocompatible graphene paper', *Adv. Mater.*, 2008, **20**, pp. 3557–3561
[20] Robinson J.T., Zalalutdinov M., Baldwin J.W., *ET AL.*: 'Wafer-scale reduced graphene oxide films for nanomechanical devices', *Nano Lett.*, 2008, **8**, pp. 3441–3445
[21] Gómez-Navarro C., Meyer J.C., Sundaram R.S., *ET AL.*: 'Atomic structure of reduced graphene oxide', *Nano Lett.*, 2010, **10**, pp. 1144–1148
[22] Nasehnia F., Mohammadpour L.S., Seifi M., *ET AL.*: 'First principles study on optical response of graphene oxides: from reduced graphene oxide to the fully oxidized surface', *Comput. Mater. Sci.*, 2016, **114**, pp. 112–120
[23] Zhao H., Aluru N.R.: 'Temperature and strain-rate dependent fracture strength of graphene', *J. Appl. Phys.*, 2010, **108**, p. 64321
[24] Zhang Y.Y., Wang C.M., Cheng Y., *ET AL.*: 'Mechanical properties of bilayer graphene sheets coupled by sp3 bonding', *Carbon*, 2011, **49**, pp. 4511–4517
[25] Wang L., Zhang Q.: 'Elastic behavior of bilayer graphene under in-plane loadings', *Curr. Appl. Phys.*, 2012, **12**, pp. 1173–1177
[26] Fonseca A.F., Liang T., Zhang D., *ET AL.*: 'Probing the accuracy of reactive and non-reactive force fields to describe physical and chemical properties of graphene-oxide', *Comput. Mater. Sci.*, 2016, **114**, pp. 236–243
[27] Paci J.T., Belytschko T., Schatz G.C.: 'Computational studies of the structure, behavior upon heating, and mechanical properties of graphite oxide', *J. Phys. Chem. C*, 2007, **111**, pp. 18099–18111
[28] Abolfath R.M., Cho K.: 'Computational studies for reduced graphene oxide in hydrogen-rich environment', *J. Phys. Chem. A*, 2012, **116**, pp. 1820–1827
[29] Kumar P.V., Bernardi M., Grossman J.C.: 'The impact of functionalization on the stability, work function, and photoluminescence of reduced graphene oxide', *ACS Nano*, 2013, **7**, pp. 1638–1645
[30] Dewapriya M.A.N., Rajapakse R.K.N.D., Nigam N.: 'Influence of hydrogen functionalization on the fracture strength of graphene and the interfacial properties of graphene–polymer nanocomposite', *Carbon*, 2015, **93**, pp. 830–842
[31] Zhang C., Dabbs D.M., Liu L., *ET AL.*: 'Combined effects of functional groups, lattice defects, and edges in the infrared spectra of graphene oxide', *J. Phys. Chem. C*, 2015, **119**, pp. 18167–18176
[32] Wang C., Peng Q., Wu J., *ET AL.*: 'Mechanical characteristics of individual multi-layer graphene-oxide sheets under direct tensile loading', *Carbon*, 2014, **80**, pp. 279–289
[33] Wei X., Mao L., Soler-Crespo R.A., *ET AL.*: 'Plasticity and ductility in graphene oxide through a mechanochemically induced damage tolerance mechanism', *Nat. Commun.*, 2015, **6**, p. 8029
[34] Lawson D.B., Beregszaszy E.J.: 'Incremental oxidation of the surface of monolayer and bilayer graphene: a computational study', *Physica E*, 2015, **68**, pp. 164–170
[35] Plimpton S.: 'LAMMPS molecular dynamics simulator'. Available at http://www.lammps.sandia.gov/2011
[36] Chenoweth K., van Duin A.C.T., Goddard W.A.: 'ReaxFF reactive force field for molecular dynamics simulations of hydrocarbon oxidation', *J. Phys. Chem. A*, 2008, **112**, pp. 1040–1053
[37] Bagri A., Mattevi C., Acik M., *ET AL.*: 'Structural evolution during the reduction of chemically derived graphene oxide', *Nat. Chem.*, 2010, **2**, pp. 581–587
[38] Fonseca A.F., Zhang H., Cho K.: 'Formation energy of graphene oxide structures: a molecular dynamics study on distortion and thermal effects', *Carbon*, 2015, **84**, pp. 365–374
[39] Stobinski L., Lesiak B., Malolepszy A., *ET AL.*: 'Graphene oxide and reduced graphene oxide studied by the XRD, TEM and electron spectroscopy methods', *J. Electron Spectrosc.*, 2014, **195**, pp. 145–154
[40] Liu X., Wen Y., Shan B., *ET AL.*: 'Combined effects of defects and hydroxyl groups on the electronic transport properties of reduced graphene oxide', *Appl. Phys. A*, 2015, **118**, pp. 885–892
[41] Mattevi C., Eda G., Agnoli S., *ET AL.*: 'Evolution of electrical, chemical, and structural properties of transparent and conducting chemically derived graphene thin films', *Adv. Funct. Mater.*, 2009, **19**, pp. 2577–2583
[42] King A., Johnson G., Engelberg D., *ET AL.*: 'Observations of intergranular stress corrosion cracking in a grain-mapped polycrystal', *Science*, 2008, **321**, pp. 382–385

doi: 10.1049/mnl.2017.0072